SAND2022-2649C

Impact of radar flightpath on synthetic aperture radar image height of focus

A. W. Doerry,* D. L. Bickel

Sandia National Laboratories, P.O. Box 5800, MS 0519, Albuquerque, NM 87185

ABSTRACT

Synthetic Aperture Radar (SAR) projects a 3-D scene's reflectivity into a 2-D image. In doing so, it generally focuses the image to a surface, usually a ground plane. Consequently, scatterers above or below the focal/ground plane typically exhibit some degree of distortion manifesting as a geometric distortion and misfocusing or smearing. Limits to acceptable misfocusing define a Height of Focus (HOF), analogous to Depth of Field in optical systems. This may be exacerbated by the radar's flightpath during the synthetic aperture data collection. HOF is very radar flightpath dependent. Some flightpaths like straight and level flightpaths will have very large HOF limits. Other flightpaths, especially those that exhibit large out-of-plane motion will have very small HOF limits, perhaps even small fractions of a meter. This paper explores the impact of various flightpaths on HOF, and discusses the conditions for increasing or decreasing HOF. We note also that HOF might be exploited for target height estimation and offer insight to other height estimation techniques.

Keywords: radar, SAR, image focus, height-of-focus

1 INTRODUCTION

Synthetic Aperture Radar (SAR) is an imaging technique that renders a 2-D image of a 3-D scene of interest.[1] Pixel values are associated with radar reflectivity. Like many imaging systems, a SAR image is typically "focused" to some surface, usually the ground, which is typically assumed to be a horizontal flat planar surface. Scatterers above or below this focused surface generally exhibit some distortions that include one or more of the following.

1. Shifting of the apparent location, in perhaps both range and azimuth (cross-range), and
2. Defocusing of the scatterer's response in the image.

The first of these is responsible for "layover," sometimes called "foreshortening," and is a geometric distortion of the apparent scatterer location. The second issue is analogous to an optical "depth of field" limitation. In SAR, it is more commonly referred to as a "Height of Focus (HOF)," or "Depth of Focus (DOF)" limitation. A number of SAR publications discuss these phenomena, including texts by Jakowatz, et al.,[2] Oliver and Quegan,[3] Curlander and McDonough,[4] and Mensa.[5] We assess the effects of scatterer height above/below the SAR image focal plane. While our principal interest here is with respect to HOF, we note that this is inextricably linked to layover as well, all related to manifestations of the same phenomenon. In addition, we briefly mention how HOF might be exploited to calculate scatterer height itself, and relate this to other scatterer height calculation techniques. This paper is an abridged summary of more detailed analysis presented in an earlier report.[6]

2 DATA MODEL

With spotlight mode SAR, including individual spotlight images that become mosaicked into stripmaps, typically each pulse is identified with a unique pulse number or index, and used in a single SAR image. The pulse index number is typically known prior to collection. This mode allows the maximum degree of motion compensation via pulse parameter

* awdoerr@sandia.gov; phone 505-845-8165; www.sandia.gov/radar

modulation, if so desired. We will calculate HOF as a misfocus due to an elevation offset of an otherwise perfectly focused point target in the image plane. The misfocus will be due to unexpected ranging errors, manifested as phase errors as a function of pulse index, due to the point target's elevation. Consequently, we expect the principal effect to be a misfocus in the azimuth, or cross-range dimension. Constant and linear phase errors will manifest as a geometric distortion, i.e. a displacement of the point target in the SAR image. Higher-order phase errors will manifest as a misfocus, or smearing of the point target response. In particular, second-order, or quadratic, phase errors will be the dominate component of the misfocusing. Our signal model is developed accordingly.

2.1 The Radar Echo Signal Model

Everything begins with a signal model. We shall assume a transmitted (TX) signal of the analytic signal form

$$x_T(t,n) = A_T \operatorname{rect}\left(\frac{t-t_n}{T_{TX}}\right)\exp\left(j\omega_{T,n}(t-t_n)\right), \tag{1}$$

where n = azimuth sample index with bounds, $-N/2 \le n < N/2$, N = total number of azimuth samples which is presumed even for convenience, t_n = reference time for the nth TX pulse, A_T = arbitrary amplitude of the TX pulse, T_{TX} = the TX pulse width, $\omega_{T,n}$ = reference center frequency for the nth pulse, and the pulse envelope function is

$$\operatorname{rect}(z) = \begin{cases} 1 & |z| \le 1/2 \\ 0 & else \end{cases}. \tag{2}$$

The received echo signal from a single point target reflector is then delayed and attenuated to

$$x_R(t,n) = A_R \operatorname{rect}\left(\frac{t-t_n-t_{s,n}}{T_{TX}}\right)\exp\left(j\omega_{T,n}(t-t_n-t_{s,n})\right), \tag{3}$$

where A_R = the received echo signal amplitude, and $t_{s,n}$ = the echo delay time for the point target scatterer.

2.2 Geometry

With a specific set of pulses defining the synthetic aperture selected, we can define a particular coordinate frame for that synthetic aperture as indicated in Figure 1.

We now define a somewhat arbitrary x,y,z coordinate frame. The xy plane is locally horizontal and containing the Scene Reference Point (SRP). The SRP defines the center or origin of the x,y,z coordinate frame. It is also sometimes referred to as the Motion Compensation Point (MCP) because real-time parameters are chosen and modulated to stabilize the echo from this point. Specific vectors in this coordinate frame are

$$\begin{aligned} &\mathbf{s} = \text{the vector from the SRP to the target scatterer point,} \\ &\mathbf{r}_{c,n} = \text{the vector from the SRP to the radar, and} \\ &\mathbf{r}_{s,n} = \mathbf{r}_{c,n} - \mathbf{s} = \text{vector from target point to the radar.} \end{aligned} \tag{4}$$

Note that $\mathbf{r}_{c,n}$ is also generally a function of pulse index n. The radar and target vectors identify the following respective Cartesian coordinates

$$\begin{aligned} &x_c, y_c, z_c = \text{the coordinate identified by } \mathbf{r}_{c,n} \text{ in the } x,y,z \text{ coordinate frame, and} \\ &s_x, s_y, s_z = \text{the coordinate identified by } \mathbf{s} \text{ in the } x,y,z \text{ coordinate frame.} \end{aligned} \tag{5}$$

The radar coordinates are related to the angles in Figure 1 as

$$x_c = \left|\mathbf{r}_{c,n}\right| \cos\psi_n \sin\alpha_n ,$$
$$y_c = -\left|\mathbf{r}_{c,n}\right| \cos\psi_n \cos\alpha_n ,$$
$$z_c = \left|\mathbf{r}_{c,n}\right| \sin\psi_n \ , \tag{6}$$

where for the *n*th pulse, α_n = the aperture angle between the radar position and the center of the synthetic aperture, ψ_n = the grazing angle with respect to horizontal at the SRP, ψ_0 = the nominal grazing angle with respect to horizontal at the SRP, generally expected at the aperture center. Note that in spite of our neglecting (for our convenience) a subscript for these individual Cartesian coordinates in Eq. (6), they are still functions of pulse index *n*.

We note that sampling angles α_n may be specified to offer processing advantages for other modes and algorithms. For example, they may be selected based on constant radar Pulse Repetition Frequency (PRF), constant angular increment, or constant increments in some function of the angle such as $\tan\alpha$. We also for convenience define the nominal range vector from the SRP to the nominal center of the synthetic aperture (APC_0) as $\mathbf{r}_{c0}$. This vector will exhibit a grazing angle of ψ_0, with a *y*-coordinate of y_0.

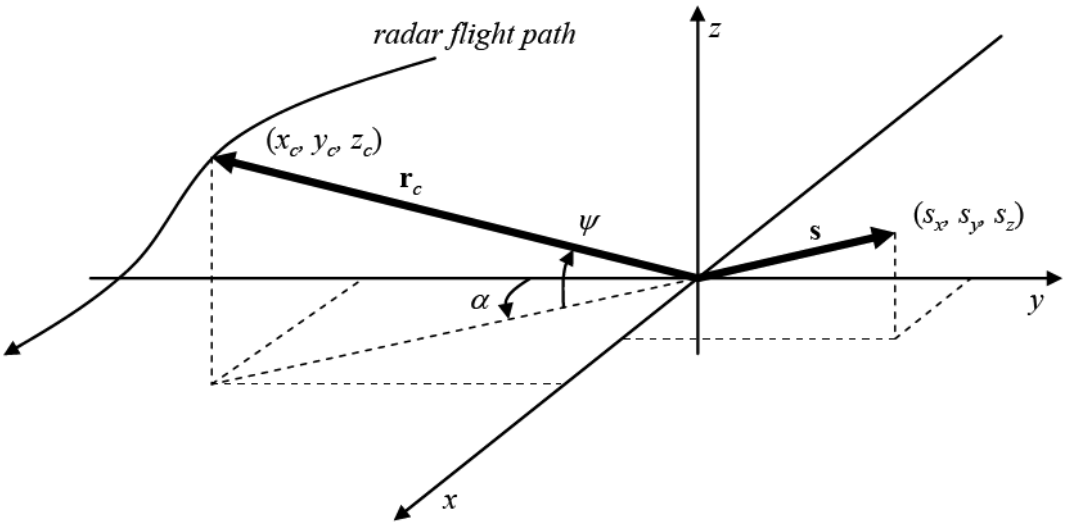

Figure 1. Radar data collection geometry.

From this geometry we identify the echo delay time as

$$t_{s,n} = \frac{2}{c}\left|\mathbf{r}_{c,n} - \mathbf{s}\right| = \frac{2}{c}\sqrt{\left|\mathbf{r}_{c,n}\right|^2 + \left|\mathbf{s}\right|^2 - 2\mathbf{r}_{c,n} \bullet \mathbf{s}} \ . \tag{7}$$

For our purposes, it is useful to stabilize the phase-history data phase response over index *n* for offsets in horizontal displacements s_x and s_y. We do this by either real-time motion compensation, or subsequent data resampling to effect

$$\omega_{T,n} = \omega_0 \frac{\cos\psi_0}{\cos\psi_n \cos\alpha_n} \ . \tag{8}$$

This is the equivalent to polar reformatting in Polar Format image formation processing.

3 MATCHED FILTER PROCESSING

The matched filter is well understood and reported in the literature. Representative texts include those by McDonough, and Whalen,[7] and Davenport and Root.[8] It maximizes the Signal-to-Noise Ratio (SNR) of its output in the presence of White Gaussian Noise (WGN). This is what SAR image formation algorithms all try to implement with various trades between image fidelity and processing ease.

We define the matched filter for a point target located with vector $\hat{\mathbf{s}}$ based on the expected response of a unit amplitude target at that location, that is

$$h\left(i,n,\hat{\mathbf{s}}\right)=\text{rect}\left(\frac{t-t_n-\frac{2}{c}\sqrt{\left|\mathbf{r}_{c,n}\right|^2+\left|\hat{\mathbf{s}}\right|^2-2\mathbf{r}_{c,n}\bullet\hat{\mathbf{s}}}}{T_{TX}}\right)\exp\left(j\omega_{T,n}\left(t-t_n-\frac{2}{c}\sqrt{\left|\mathbf{r}_{c,n}\right|^2+\left|\hat{\mathbf{s}}\right|^2-2\mathbf{r}_{c,n}\bullet\hat{\mathbf{s}}}\right)\right). \tag{9}$$

The phase of the matched filter output will then be

$$\Phi'_V\left(i,n,\hat{\mathbf{s}}\right)=\frac{2}{c}\omega_0\cos\psi_0\left[\frac{\sqrt{\left|\mathbf{r}_{c,n}\right|^2+\left|\mathbf{s}\right|^2-2\mathbf{r}_{c,n}\bullet\mathbf{s}}-\sqrt{\left|\mathbf{r}_{c,n}\right|^2+\left|\hat{\mathbf{s}}\right|^2-2\mathbf{r}_{c,n}\bullet\hat{\mathbf{s}}}}{\cos\psi_n\cos\alpha_n}\right]. \tag{10}$$

We will sample the synthetic aperture by selecting sampling angles at $\tan\alpha_n=d\alpha\, n$, where $d\alpha$ = constant. We will then generally find that Eq. (10) can be expanded into a series of the form

$$\Phi'_V\left(i,n,\hat{\mathbf{s}}\right)=\frac{2}{c}\omega_0\cos\psi_0\left[\left(s_y-\Delta_y-\hat{s}_y\right)-\left(s_x-\Delta_x-\hat{s}_x\right)d\alpha\, n+F_2\left(s_z\right)\left(d\alpha\, n\right)^2+\textit{higher order terms}\right], \tag{11}$$

where Δ_y = shift in the apparent location of s_y, Δ_x = shift in the apparent position of s_x, and $F_2\left(s_z\right)$ = coefficient of the quadratic misfocus term due to scatterer height. The shifting in the apparent position of the scatterer due to scatterer height is a geometric distortion; the aforementioned layover effect. Our interest herein remains mainly on the terms that cause misfocus.

In the neighborhood of the SRP, the quadratic (in index *n*) phase error term will be mainly due to s_z. Higher order phase error terms will also generally exist, but are typically dominated by the quadratic phase error term, justifying limiting our attention to a second-order expansion. In any case, these phase error terms cause a misfocus in the matched filter output, that increases as the magnitude of s_z increases.

4 IMPACT OF RADAR FLIGHTPATH

We now examine how some typical flightpaths impact the contribution of scatterer height on the radar data model, and ultimately the matched filter with phase given in Eq. (11). To facilitate the following discussion, we note that the azimuth resolution of the SAR image is nominally calculated as

$$\rho_x=\frac{\lambda_0}{2\cos\psi_0\, N\, d\alpha}, \tag{12}$$

where $\lambda_0=2\pi c/\omega_0$ = nominal wavelength. We are ignoring any effects of window taper functions during processing.

We define the limit of acceptable misfocus as the condition that the peak quadratic phase error reaches some limit. We write this as

$$\frac{2}{c}\omega_0 \cos\psi_0 \left[\left| F_2\left(s_z\right) \right| \left(d\alpha\, n\right)^2 \right] \Bigg|_{\substack{n=N/2 \\ s_z = s_{z,\max}}} = \phi_{\text{limit}} \quad , \tag{13}$$

where ϕ_{limit} = the acceptable quadratic phase error limit, and $s_{z,\max}$ = the height error that achieves this phase error limit, i.e. the HOF. A common limit for acceptable quadratic phase error is $\phi_{\text{limit}} = \pi/2$. We concede that this is somewhat arbitrary, and note that some sources might use other criteria.

Rearranging Eq. (13) with some substitutions lets us calculate

$$\left| F_2\left(s_{z,\max}\right) \right| = \left(\frac{4\phi_{\text{limit}}}{\pi} \right) \cos\psi_0 \frac{{\rho_x}^2}{\lambda_0} \quad . \tag{14}$$

The task is to find the $s_{z,\max}$ that satisfies this equation, that value being the HOF.

4.1 Broadside Straight Line Flightpath

Now consider a level broadside straight line flightpath as illustrated in the plan view of Figure 2. In this geometry, the range and grazing angle varies along the flightpath. We identify

$$\begin{aligned} &\left|\mathbf{r}_{c,n}\right| = \left|\mathbf{r}_{c0}\right| \sqrt{1 + \cos^2\psi_0 \left(d\alpha\, n\right)^2} \text{ , and} \\ &\cos\psi_n = \left|\mathbf{r}_{c0}\right| \cos\psi_0 \sqrt{1 + (d\alpha\, n)^2} \Big/ \left|\mathbf{r}_{c,n}\right| \text{, for all } n. \end{aligned} \tag{15}$$

An expansion of Eq. (10) after having incorporated this flightpath allows us to estimate the principal behaviors of the elements in Eq. (11) as

$$\begin{aligned} &\Delta_y \approx s_z \tan\psi_0 \text{ ,} \\ &\Delta_x = 0 \text{ , and} \\ &F_2\left(s_z\right) \approx \frac{s_z^2 \tan^2\psi_0}{2\left|\mathbf{r}_{c0}\right| \left(1 + \tan^2\psi_0\right)^{3/2}} . \end{aligned} \tag{16}$$

Consequently, we observe from this that the matched filter output will peak at a location

$$\left(\hat{s}_x \text{ , } \hat{s}_y \right) = \left(\quad s_x \quad \text{, } \quad s_y - s_z \tan\psi_0 \quad \right) . \tag{17}$$

Using Eq. (14), we calculate the HOF by solving for

$$s_{z,\max} = \sqrt{\left(\frac{8\phi_{\text{limit}}}{\pi} \right) \left(\frac{\left|\mathbf{r}_{c0}\right| \left(1 + \tan^2\psi_0\right)^{3/2} \cos\psi_0}{\tan^2\psi_0} \right) \frac{{\rho_x}^2}{\lambda_0}} \quad . \tag{18}$$

Example

We consider an example with the following operating parameters.

$|\mathbf{r}_{c0}|$ = 10 km, $\psi_0 = \pi/6$ rad. (30 deg.),
ρ_x = 0.1 m, λ_0 = 18 mm (Ku-band),
$\phi_{\text{limit}} = \pi/2$ rad. (90 deg.). (19)

From this we calculate the HOF as $s_{z,\max}$ = 298 m. That is, with the SAR image focused to a ground plane at $s_z = 0$, then any scatterer above or below this by more than 298 m will exhibit a greater-than $\pi/2$ radian quadratic phase error.

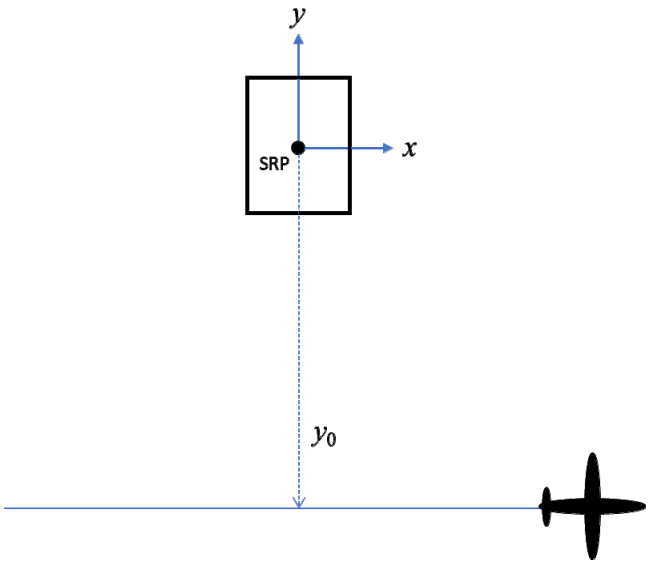

Figure 2. Plan view of broadside straight line flightpath.

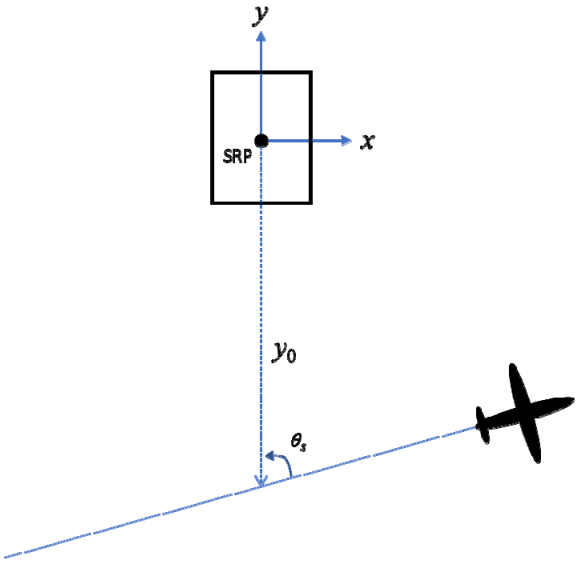

Figure 3. Plan view of squinted straight-line flightpath.

4.2 Squinted Straight Line

Now consider a level squinted straight line flightpath as illustrated in the plan view of Figure 3. We define the squint angle as

$$\theta_s \text{ = squint angle as projected in the ground plane.} \tag{20}$$

In this geometry, the range and grazing angle varies along the flightpath. We identify

$$\begin{aligned} &\left|\mathbf{r}_{c,n}\right| = \left|\mathbf{r}_{c0}\right|\sqrt{\sin^2\psi_0 + \beta^2}\ , \text{ and} \\ &\tan\psi_n = \sin\psi_0/\beta \ \text{ for all } n, \end{aligned} \tag{21}$$

where we employ the intermediate parameter

$$\beta = \sqrt{\left(1+\left(\,d\alpha\ n\right)^2\right)}\left(\cos\psi_0\tan\theta_s\ \right)\Big/\left(\tan\theta_s + d\alpha\ n\right). \tag{22}$$

An expansion of Eq. (10) after having incorporated this flightpath allows us to estimate the principal behaviors of the elements in Eq. (11) as

$$\begin{aligned} &\Delta_y \approx s_z\tan\psi_0\ , \\ &\Delta_x \approx -s_z\tan\psi_0\cot\theta_s\ , \text{ and} \\ &F_2\left(s_z\right) \approx \frac{s_z^2\tan^2\psi_0\left(\left(1+\tan^2\psi_0\right)\tan^2\theta_s + \tan^2\psi_0 - 3\right)}{2\left|\mathbf{r}_{c0}\right|\left(1+\tan^2\psi_0\right)^{5/2}\tan^2\theta_s}. \end{aligned} \tag{23}$$

Consequently, we observe from this that the matched filter output will peak at a location

$$\left(\ \hat{s}_x\ ,\ \hat{s}_y\ \right) = \left(\ \ s_x + s_z\tan\psi_0\cot\theta_s\ \ ,\ \ s_y - s_z\tan\psi_0\ \ \right). \tag{24}$$

Note that we now have layover in the azimuth (cross-range) direction as well, that depends on the squint angle of the collection. Using Eq. (14), we calculate the HOF to be

$$s_{z,\max} = \sqrt{\left(\frac{8\phi_{\text{limit}}}{\pi}\right)\left(\frac{\left|\mathbf{r}_{c0}\right|\left(1+\tan^2\psi_0\right)^{5/2}\tan^2\theta_s\cos\psi_0}{\tan^2\psi_0\left(\left(1+\tan^2\psi_0\right)\tan^2\theta_s + \tan^2\psi_0 - 3\right)}\right)\frac{\rho_x{}^2}{\lambda_0}}\ . \tag{25}$$

Note that as $\theta_s \to \pi/2$, or broadside, then Eq. (25) approaches Eq. (18), as we might expect.

Example

We consider an example with the operating parameters given in Eq. (19), but at a squint angle of

$$\theta_s = \pi/3 \text{ rad. (60 deg.).} \tag{26}$$

From this we calculate the HOF as $s_{z,\max}$ = 516 m. That is, with the SAR image focused to a ground plane at $s_z = 0$, then any scatterer above or below this by more than 516 m will exhibit a greater-than $\pi/2$ radian quadratic phase error. The value for $s_{z,\max}$ may be more or less, depending on squint angle and/or grazing angle.

4.3 Broadside Circular Orbit

Consider a level broadside circular orbit flightpath as illustrated in the plan view of Figure 4. In this geometry, the grazing angle is held constant. Consequently, we identify

$$\begin{aligned} &\psi_n = \psi_0 \text{, and} \\ &\left|\mathbf{r}_{c,n}\right| = \left|\mathbf{r}_{c0}\right| \text{, for all } n. \end{aligned} \tag{27}$$

An expansion of Eq. (10) after having incorporated this flightpath allows us to estimate the principal behaviors of the elements in Eq. (11) as

$$\begin{aligned} &\Delta_y \approx s_z \tan\psi_0 \text{,} \\ &\Delta_x = 0 \text{, and} \\ &F_2\left(s_z\right) \approx \frac{\tan\psi_0}{2} s_z \text{.} \end{aligned} \tag{28}$$

Consequently, we observe from this that the matched filter output will peak at a location

$$\left(\hat{s}_x \text{ , } \hat{s}_y\right) = \left(s_x \text{ , } s_y - s_z \tan\psi_0 \right) . \tag{29}$$

Using Eq. (14), we calculate the HOF to be

$$s_{z,\max} = \left(\frac{8\phi_{\text{limit}}}{\pi}\right)\left(\frac{\cos^2\psi_0}{\sin\psi_0}\right)\frac{\rho_x^{\,2}}{\lambda_0} \text{ .} \tag{30}$$

Example

We consider an example with the operating parameters given in Eq. (19).

From this we calculate the HOF as $s_{z,\max}$ = 3.33 m. That is, with the SAR image focused to a ground plane at $s_z = 0$, then any scatterer above or below this by more than 3.33 m will exhibit a greater-than $\pi/2$ radian quadratic phase error. This is considerably more restrictive than the previous examples, which calculated $s_{z,\max}$ at several hundred meters. This would be noticeable even for moderate topography in a scene.

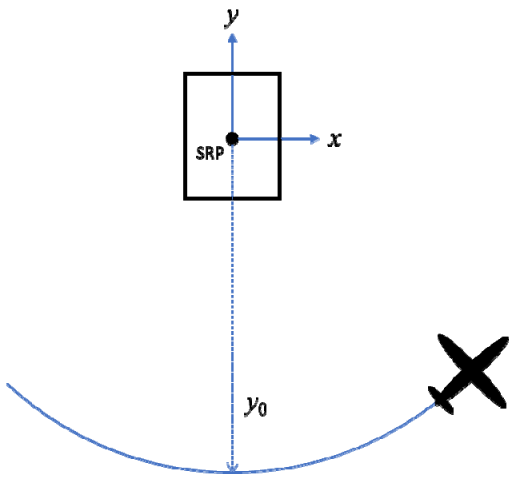

Figure 4. Plan view of circular orbit flightpath.

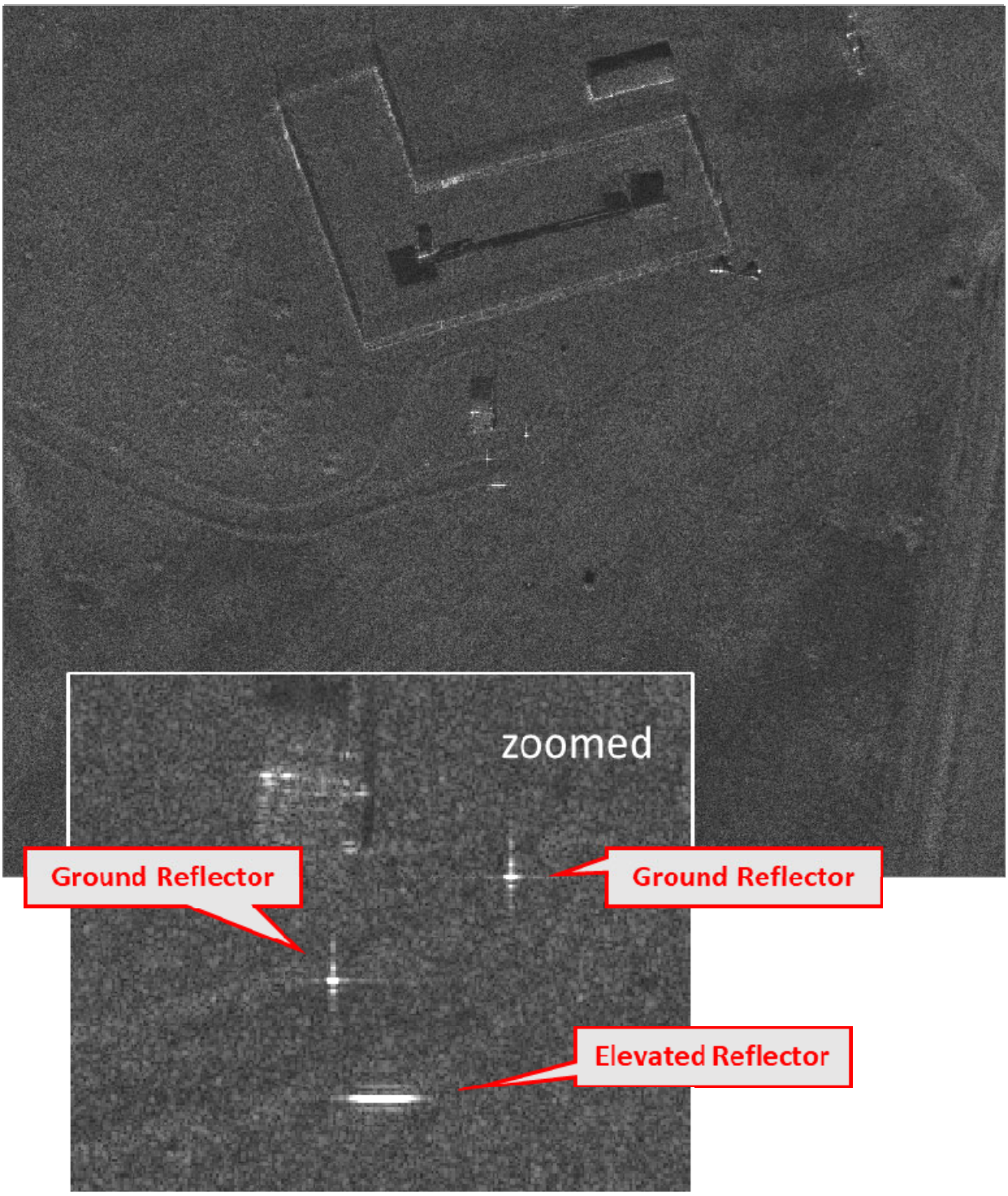

Figure 5. Example of defocusing due to elevated target reflector. Elevated reflector is on a pole about 16 m above the ground. Image was collected with a Sandia Ku-band testbed radar, flying an approximately circular orbit flightpath, operating at 4 km range, 29.8 degree grazing angle, 0.1 m resolution. Scene is of a facility on Kirtland AFB, Albuquerque, New Mexico, USA. HOF is calculated to be about 3.33 m.

4.4 Exaggerated Curvature – Inside Turn

Consider a level flightpath with an exaggerated curvature as illustrated in the plan view of Figure 6. The flightpath is an offset circular orbit, but about a point towards but much nearer than the SRP, with a radius of curvature ρ. In this geometry, the instantaneous layover changes considerably during the flightpath. Consequently, we identify

$$\begin{aligned} &\left|\mathbf{r}_{c,n}\right| = \left|\mathbf{r}_{c0}\right|\sqrt{\sin^2\psi_0 + \beta^2} \text{ , and} \\ &\tan\psi_n = \sin\psi_0/\beta \text{ for all } n, \end{aligned} \tag{31}$$

where we employ the intermediate parameter

$$\beta = \left(\cos\psi_0 + \frac{\rho}{\left|\mathbf{r}_{c0}\right|}\left(\sqrt{1-\left(d\alpha\, n\right)^2\left(\left(\frac{\left|\mathbf{r}_{c0}\right|\cos\psi_0}{\rho} - 1 \right)^2 - 1 \right)} - 1 \right) \right) \Bigg/ \sqrt{1+\left(d\alpha\, n\right)^2} \ . \tag{32}$$

An expansion of Eq. (10) after having incorporated this flightpath allows us to estimate the principal behaviors of the elements in Eq. (11) as

$$\begin{aligned} &\Delta_y \approx s_z \tan\psi_0 \text{ ,} \\ &\Delta_x = 0 \text{ , and} \\ &F_2\left(s_z\right) \approx -\frac{\sin\psi_0}{2\left(\rho/\left|\mathbf{r}_{c0}\right|\right)} s_z \text{ .} \end{aligned} \tag{33}$$

Consequently, we observe from this that the matched filter output will peak at a location

$$\left(\hat{s}_x \text{ , } \hat{s}_y \right) = \left(\ s_x \ \text{ , } \ s_y - s_z \tan\psi_0 \ \right) \ . \tag{34}$$

Using Eq. (14), we calculate the HOF to be

$$s_{z,\max} = \left(\frac{8\phi_{\text{limit}}}{\pi} \right)\left(\frac{\rho}{\left|\mathbf{r}_{c0}\right|} \right)\cot\psi_0 \, \frac{{\rho_x}^2}{\lambda_0} \ . \tag{35}$$

Note that the case where $\rho = \left|\mathbf{r}_{c0}\right|\cos\psi_0$ devolves to Eq. (30), as the geometry devolves to the example in Section 4.3. However, clearly as the radius of curvature of the flightpath decreases, so too does the HOF decrease.

Example

We consider an example with the operating parameters given in Eq. (19), but with

$$\rho/\left|\mathbf{r}_{c0}\right| = 0.1 \text{ .} \tag{36}$$

From this we calculate the HOF as $s_{z,\max}$ = 0.38 m. That is, with the SAR image focused to a ground plane at $s_z = 0$, then any scatterer above or below this by more than 0.38 m will exhibit a greater than $\pi/2$ radian quadratic phase error. This is considerably more restrictive than the circular orbit in Section 4.3, which calculated $s_{z,\max}$ at 3.33 meters. This would be highly noticeable even for moderate topography in a scene.

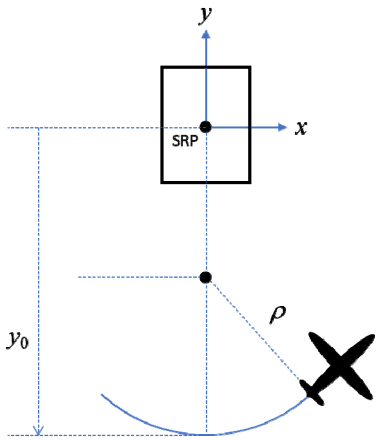

Figure 6. Plan view of offset circular orbit flightpath, with turn towards SRP.

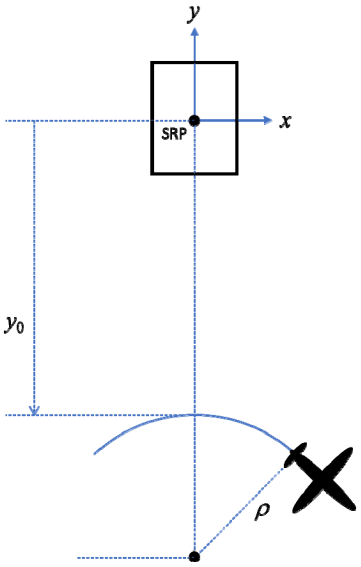

Figure 7. Plan view of offset circular orbit flightpath, with turn away from SRP.

4.5 Exaggerated Curvature – Outside Turn

Consider a level flightpath with an exaggerated curvature as illustrated in the plan view of Figure 7. The flightpath is an offset circular orbit, but about a point away from but much nearer than the SRP. In this geometry, the instantaneous layover changes considerably during the flightpath. Consequently, we identify

$$\begin{aligned} &\left|\mathbf{r}_{c,n}\right| = \left|\mathbf{r}_{c0}\right|\sqrt{\sin^2\psi_0 + \beta^2}\ , \text{and} \\ &\tan\psi_n = \sin\psi_0/\beta \ \text{ for all } n, \end{aligned} \tag{37}$$

where we employ the intermediate parameter

$$\beta = \left(\cos\psi_0 + \frac{\rho}{\left|\mathbf{r}_{c0}\right|}\left(\sqrt{1-(d\alpha n)^2\left(\left(\frac{\left|\mathbf{r}_{c0}\right|\cos\psi_0}{\rho}+1 \right)^2 - 1 \right)} - 1 \right) \right) \Bigg/ \sqrt{1+(d\alpha n)^2}\ . \tag{38}$$

An expansion of Eq. (10) after having incorporated this flightpath allows us to estimate the principal behaviors of the elements in Eq. (11) as

$$\Delta_y \approx s_z \tan\psi_0 ,$$
$$\Delta_x = 0 , \text{ and}$$
$$F_2(s_z) \approx \left(\frac{\sin\psi_0}{2(\rho/|\mathbf{r}_{c0}|)} \right) s_z . \tag{39}$$

Consequently, we observe from this that the matched filter output will peak at a location

$$\left(\hat{s}_x , \hat{s}_y \right) = \left(\; s_x \; , \; s_y - s_z \tan\psi_0 \; \right) . \tag{40}$$

Using Eq. (14), we calculate the HOF to be

$$s_{z,\max} = \left(\frac{8\phi_{\text{limit}}}{\pi} \right) \left(\frac{\rho}{|\mathbf{r}_{c0}|} \right) \cot\psi_0 \, \frac{{\rho_x}^2}{\lambda_0} \; . \tag{41}$$

Note that this is the same as Eq. (35) in the previous example, where the radius of curvature of the flightpath was the same, but in the other direction. Again, however, clearly as the radius of curvature of the flightpath decreases, so too does the HOF decrease.

Example

We consider an example with the operating parameters given in Eq. (19), but with

$$\rho/|\mathbf{r}_{c0}| = 0.1 , \tag{42}$$

which are the same as the example in the previous section. From this we calculate the HOF as $s_{z,\max} = 0.38$ m. That is, with the SAR image focused to a ground plane at $s_z = 0$, then any scatterer above or below this by more than 0.38 m will exhibit a greater than $\pi/2$ radian quadratic phase error, again more restrictive than the orbit in Section 4.3.

4.6 Comments

We to offer some comments and observations.

- Layover and HOF are inextricably linked. They are manifestations of the same phenomenon, namely a phase function resulting from a non-zero scatterer height above the SAR image focal plane or surface. Constant and linear terms across a synthetic aperture cause layover in range and azimuth respectively, whereas higher-order terms cause a misfocus that worsens with height magnitude. The phase functions that manifest as layover and misfocus due to scatterer height, result from ranges between radar and scatterer behaving differently than if the scatterer were at the focal plane height. Consequently, HOF is all about nonlinear range variations due to height offset with respect to the focused or reference ground level during the synthetic aperture.
- We may conclude that a straight-line flightpath offers minimum sensitivity to scatterer height, that is a large HOF. A label such as “good” or “bad” depends on whether we desire a large HOF or not. For now, we state without elaboration that associating a large or small HOF with labels such as “good” or “bad” depends on the specific application we are considering.
- We may conjecture that if a nonlinear phase function due to an elevated scatterer causes a smearing in the SAR image, then anything that causes a smearing in the SAR image of an elevated scatterer with respect to one at the reference ground level is likely due to a nonlinear phase function, and will ultimately lead to a HOF limit. Such a smearing might result from the instantaneous layover direction changing during the synthetic aperture. So, we might infer that flightpaths that cause larger changes in instantaneous layover direction during a synthetic aperture will likely more severely reduce HOF. Such flightpaths will necessarily be curved or bent in some fashion, and definitely not be linear or straight-line flightpaths.

- All of our previous examples assumed the radar flying in a horizontal plane significantly above the SRP. All curvature in our examples was within this horizontal elevated plane. Consequently, no single planar surface could contain the entire flightpath as well as the SRP. If we tilt the plane down to contain the SRP, thereby becoming a "slant plane," then the flightpath necessarily cannot be entirely contained in the slant plane. The flightpath then exhibits "out of plane" motion with respect to the slant plane. HOF can in fact be assessed in terms of this out of plane motion.[2]
- Curvature within the slant plane will not constrain HOF like curvature that results in out-of-plane motion. This can be seen by examining any of the curved flightpath examples, by letting the grazing angle go to very small values. As it does so, the HOF grows correspondingly. This is regardless of how much curvature is 'within' the slant plane.
- We opine that operationally, airborne radar flightpaths are likely to be constrained to a constant altitude, thereby limited to achieving their out-of-plane motion with horizontal curvature, i.e. turning. They will look more like the examples previously given than to exhibit curved or bent elevation profiles. However, constant-altitude data collection is not guaranteed. In any case, except for pathological cases, the more curvature our flightpath exhibits, the smaller is the HOF.

5 EXPLOITING HOF FOR HEIGHT ESTIMATION

As previously stated, associating a large or small HOF with labels such as "good" or "bad" depends on the specific application we are considering. While we generally desire a presentation quality SAR image to be one where all parts of the image are in focus regardless of topography, implying a large HOF, we stipulate that there are other exploitation techniques that strongly desire a relatively small HOF. This is especially true for scatterer height estimation, and more generally geolocation.

The basic premise for height estimation is that by measuring the amount of misfocus, we may calculate a scatterer's height above the SRP that must have caused the misfocus. The more pronounced the misfocus, the easier it should be to calculate height with accuracy and precision. While this may not be expected to give equivalent results to more familiar techniques such as SAR Interferometry, or Stereo SAR, neither does it require an antenna with multiple phase centers (or equivalent), or multiple passes, or multiple SAR images. Nevertheless, there are strong relationships between exploiting HOF for height estimation and other height estimation techniques. All rely on target displacement in SAR data due to height offset, either within or across synthetic apertures, essentially a parallax effect, even if only observable in the phase.

Several papers have been written about estimating scatterer height from curvilinear apertures. Most notable are papers by Knaell,[9,10,11,12,13] and Knaell and Cardillo.[14] However, others have also contributed to this area.[2,15,16,17,18,19,20,21]

6 SUMMARY & CONCLUSIONS

We offer and repeat some key points.

- SAR attempts to focus scattering locations on some surface, typically a horizontal plane centered on some ground-level scene reference point. Focusing involved compensating for radar motion along its flightpath during a synthetic aperture.
- Scattering locations above or below this surface will exhibit deleterious effects due to their relative range variations not being properly compensated; the result being phase errors as a function of flightpath sampling locations. Constant and linear phase errors will result in range and azimuth displacements known as "layover." Higher-order phase errors will result in misfocus of the scatterer. Higher-order terms are typically dominated by the quadratic term.
- A limit on allowable focus degradation will result in a limit on scatterer offset from the focus plane. The vertical offset that reaches this degradation limit is termed the Height of Focus (HOF) for the image.
- HOF is very radar flightpath dependent. Some flightpaths like straight and level flightpaths will have very large HOF limits. Other flightpaths, especially those that exhibit large out-of-plane motion will have very small HOF limits, perhaps even small fractions of a meter.

- HOF might be exploited for scatterer height estimation. In any case, the physics of HOF calculation are very related to other height estimation techniques.

ACKNOWLEDGEMENTS

Sandia National Laboratories is a multimission laboratory managed and operated by National Technology & Engineering Solutions of Sandia LLC, a wholly owned subsidiary of Honeywell International Inc. for the U.S. Department of Energy's National Nuclear Security Administration under contract DE-NA0003525.

REFERENCES

[1] Armin W. Doerry, Fred M. Dickey, "Synthetic Aperture Radar," *Optics & Photonics News (OPN)*, November, 2004.
[2] Charles V. Jakowatz Jr., Daniel E. Wahl, Paul H. Eichel, Dennis C. Ghiglia, Paul A. Thompson, *Spotlight-Mode Synthetic Aperture Radar: A Signal Processing Approach*, ISBN 0-7923-9677-4, Kluwer Academic Publishers, 1996
[3] Chris Oliver, Shaun Quegan, *Understanding Synthetic Aperture Radar Images*, ISBN: 0-89006-850-X, Artech House, Inc., 1998.
[4] John C. Curlander, Robert N. McDonough, *Synthetic Aperture Radar, Systems & Signal Processing*, ISBN 0-471-85770-X, John Wiley & Sons, 1991.
[5] Dean L. Mensa, *High Resolution Radar Cross-Section Imaging*, ISBN: 0-89006-289-3, Artech House, Inc., 1991.
[6] Armin W Doerry, Douglas L Bickel, *Synthetic Aperture Radar Height of Focus*, Sandia National Laboratories Report SAND2021-0144, January 2021.
[7] Robert N. McDonough, Anthony D. Whalen, *Detection of Signals in Noise – Second Edition*, ISBN 0-12-744852-7, Academic Press, 1995.
[8] Wilbur B. Davenport, Jr., William L. Root, *An Introduction to the Theory of Random Signals and Noise*, ISBN 0-87942-235-1, IEEE Press, 1987.
[9] Kenneth Knaell, "Three-dimensional SAR from practical apertures," In *Radar/Ladar Processing and Applications*, vol. 2562, pp. 31-41, International Society for Optics and Photonics, 1995.
[10] Kenneth Knaell, "Advances in three-dimensional SAR from practical apertures," In *Radar Processing, Technology, and Applications*, vol. 2845, pp. 183-193, International Society for Optics and Photonics, 1996.
[11] Kenneth Knaell, "Advances in three-dimensional SAR from curvilinear apertures," *Radar Processing, Technology, and Applications II*, vol. 3161, pp. 178-184, International Society for Optics and Photonics, 1997.
[12] Kenneth Knaell, "Progress in three-dimensional SAR from curvilinear apertures," In *Radar Processing, Technology, and Applications III*, vol. 3462, pp. 110-121, International Society for Optics and Photonics, 1998.
[13] Kenneth Knaell, "Three-dimensional SAR from curvilinear apertures," In *Proceedings of the 1996 IEEE national Radar conference*, pp. 220-225, IEEE, 1996.
[14] K. K. Knaell, G. P. Cardillo, "Radar tomography for the generation of three-dimensional images," *IEE Proceedings-Radar, Sonar and Navigation*, Vol. 142, No. 2, pp. 54-60, 1995.
[15] Jian Li, Zhaoqiang Bi, Z-S. Liu, Kenneth Knaell, "Use of curvilinear SAR for three-dimensional target feature extraction," *IEE Proceedings-Radar, Sonar and Navigation*, Vol. 144, No. 5, pp. 275-283, 1997.
[16] Ren Xiaozhen, Yang Ruliang, "A method for CLSAR 3-D imaging based on backprojection and beamforming," In *2009 2nd Asian-Pacific Conference on Synthetic Aperture Radar*, pp. 1022-1025, IEEE, 2009.
[17] Liu Xiangle, Yang Ruliang, "Study of composite mode curvilinear SAR," In *2006 CIE International Conference on Radar*, pp. 1-4, IEEE, 2006.
[18] Zhigang Su, Yingning Peng, Xiutan Wang, "Evaluation of the aperture in the curvilinear SAR," In *2006 CIE International Conference on Radar*, pp. 1-4, IEEE, 2006.
[19] Zhigang Su, Guiying Liu, Yingning Peng, Renbiao Wu, Ruihua Liu, "RCB-based imaging method for 3-D target via curvilinear SAR," In *2008 9th International Conference on Signal Processing*, pp. 2368-2371, IEEE, 2008.
[20] Zhigang Su, Yue Wang, Renbiao Wu, Yingning Peng, "Use of large curvilinear synthetic aperture for 3-D target imaging," pp. 145-145, 2009.
[21] Ruizhi Hu, Rui Min, Feng Zuo, Yiming Pi, "An algorithm for persistent imaging of curvilinear video SAR," In *2018 IEEE Radar Conference (RadarConf18)*, pp. 0023-0028, IEEE, 2018.